Dependence of the Enhanced Optical Scattering Efficiency Relative to That of Absorption for Gold Metal Nanorods on Aspect Ratio, Size, End-Cap Shape, and Medium Refractive Index

Kyeong-Seok Lee[†] and Mostafa A. El-Sayed*

Laser Dynamics Laboratory, School of Chemistry and Biochemistry, Georgia Institute of Technology, Atlanta, Georgia 30332-0400

Received: August 5, 2005; In Final Form: August 29, 2005

The current intense interest in the properties of plasmonic nanostructures for their applications in chemical and biochemical sensors, medical diagnostics and therapeutics, and biological imaging is fundamentally based on their enhanced optical absorption and scattering properties. In this study, the optical extinction, absorption, and scattering efficiencies were calculated as a function of shape definition, aspect ratio, surrounding medium, and material selection. The discrete dipole approximation method was used, which is known to be a very useful and versatile computational tool for particles with any arbitrary shape. Relative contribution of scattering to the total extinction for the longitudinal mode was found to be significantly dependent on the aspect ratio of the nanorod in a somewhat complex manner, different from a typical linear relationship for the resonance wavelength. A slight elongation of Au nanosphere gives rise to a drastic increase in the relative scattering efficiency, which eventually reaches a maximum and begins to decrease with further increase in the aspect ratio. This is ascribed to the increasing absorptive contribution from the larger imaginary dielectric function of the metal particle in the longer wavelength region where the red-shifted excitation of the longitudinal resonance mode occurs. For transverse mode exhibiting the blue-shift in the resonance peak, on the contrary, the absorption efficiency is relatively enhanced compared to the scattering efficiency with increasing aspect ratio. This is thought to result from the dominant effect of the interband transition present in this wavelength region. Besides the dependence of plasmonic characteristics on the aspect ratio of nanorod, the DDA results for a small change of the end-cap shape and the index of the surrounding medium lead us to conclude that there exist two competing key factors: a weighting factor assigned to the shape parameter and the dielectric function of the metal particle, which control the relative enhancement in the scattering and absorption as well as the linearity of resonance wavelength with regard to the aspect ratio.

Introduction

Plasmonic metal nanostructures have unique electronic, catalytic, and optical characteristics.[1−3] Among these, the optical resonance properties of metal nanoparticles have been of scientific interest for centuries since first being recognized by Faraday,[4] who tried to discuss the metal precipitates having the beautiful color of stained glasses. These nanoparticles have practical value in many applications such as chemical and biochemical sensors, medical diagnostics and therapeutics, biological imaging, and nanophotonics.[5−9]

When the dimension of metal nanoparticles is small enough compared to the wavelength of incident light, surface plasmon can be excited due to a collective motion of free electrons in the metal nanoparticle that resonantly couples with the oscillating electric field of the light. As a result of the surface plasmon excitation, strong enhancements of the absorption, scattering, and local electric field around the metal particles arise and the feature strongly depends on particle size, shape, type of materials, and the local environment. This is the fundamental source for their useful applications mentioned above.

Optical absorption and scattering have dominant effects at different size regions, which can be used in certain applications. The change in the strong surface plasmon absorption (SPA) maximum has been used in sensor applications, while the strong scattering is useful in imaging methods to detect attached biosystems. For example, recently, gold nanospheres were conjugated to the antibody of an antigen present only at the surface of cancer cells, but not the healthy ones. Thus, using simple microscopy, light scattering from the gold nanoparticles on the surface of the cancer cells can be imaged and used as a sensitive diagnostic method.[10] In general, optical scattering, significant for the particles larger than a few tens of nanometers, gives a more efficient detection scheme for monitoring the local environments of single particle plasmon. For sensor and other diagnostic applications, absorption is the desired method. Therefore, it is very important to understand how the optical absorption and scattering depend on the particle's geometry and the material selection, and to find a way to control their relative contribution for the selected application. From the viewpoint of optical scattering, metal nanorods have attracted additional attention due to their higher tunability of resonance frequency. For applications in biology, the laser light needs to penetrate human tissue. This requires the use of lasers with 800−900 nm wavelengths.[11,12] If nanoparticles are used for imaging or therapeutic purposes, their scattering or absorption maximum has to be in this wavelength region. Thus the ability to tune the resonance wavelength of the nanoparticle as well as its ability

* Corresponding author. E-mail: mostafa.el-sayed@chemistry.gatech.edu.
[†] Permanent address: Thin Film Materials Research Center, Korea Institute of Science and Technology, Seoul 136-780, Korea.

10.1021/jp054385p CCC: $30.25
Published on Web 10/07/2005

to enhance the scattering or absorption, depending on the application, becomes extremely important in this field of nanotechnology. Nanorods are very important in this field. The change in the aspect ratio is known to change the longitudinal wavelength maximum of nanorods.[13−17] However, the effect of the aspect ratio change on the relative efficiencies of scattering and absorption has not yet been carefully examined. Only minor discussions[18] have been reported on how the absorption and scattering contributions depend on the aspect ratio of the nanorod and the type of materials used.

Maxwell's equations for the optical response of metal nanoparticles to an electromagnetic field of light were first solved analytically for a homogeneous isotropic sphere by Mie[19] in 1908. Although many extensions of Mie theory have been made for covering different aspects including magnetic and coated spheres,[20,21] this analytical method has a fundamental limitation that the exact solutions are restricted only to highly symmetric particles such as spheres and spheroids. A separation of variables approach similar to Mie theory was applied in a spheroidal coordinate system by Asano and Yamamoto[22] and further implemented by Voshchinnikov and Farafonov.[23] For other nonspherical particles, numerical approximate methods are generally required and there are a lot of computational methods that have been developed in recent decades based on more advanced scattering theories. These include the T-matrix method,[24] the generalized multipole technique (GMT),[25] the discrete dipole approximation (DDA),[26] and the finite different time domain (FDTD) method.[27] The first two methods can be classified as surface-based methods where only the particle's surface is discretized and solved numerically. The latter methods are referred to as volume-based methods where the entire volume is discretized.

DDA is a finite element method originally proposed by Purcel and Pennypacker[26] for application to the scattering problem of nonmetallic interstellar dust particles, which has been regarded as one of the most powerful and flexible electrodynamic methods for computing the optical scattering of particles with an arbitrary geometry since a significant implementation by Draine and Flatau.[28] Recently, Schatz and co-workers[29−31] proved that the DDA is suited for optical calculations of metallic systems with different geometries and environments through the extensive studies on the extinction spectrum and the local electric field distribution in metal particles.

In this study, we report a systematic investigation of the relative contribution of optical absorption and scattering to the total extinction of metal nanorod by adopting the DDA code developed by Draine and Flatau.[28] The exact shape of the nanorods is considered here compared to the ellipsoidal approximation. The effect of geometrical factors, such as the aspect ratio and the end-cap shape factor as well as the particle size and the surrounding medium on the optical scattering, both for longitudinal and transverse modes, is discussed with regard to the dielectric function behavior of the metal particles.

Application of DDA

In the DDA method, a target particle of interest is geometrically reproduced by a cubic array of virtual N-point dipoles with polarizabilities α_i located at positions $\boldsymbol{r}_i$. The polarization of each dipole, $\boldsymbol{P}_i$, is then described under the electric field at the respective position by

$$\boldsymbol{P}_i = \alpha_i \boldsymbol{E}_{\mathrm{loc}}(\boldsymbol{r}_i) \tag{1}$$

where $\boldsymbol{E}_{\mathrm{loc}}$ is the sum of the incident field and the contribution from all other $N-1$ dipoles:

$$\boldsymbol{E}_{\mathrm{loc}}(\boldsymbol{r}_i) = \boldsymbol{E}_{\mathrm{inc},i} + \boldsymbol{E}_{\mathrm{other},i} = \boldsymbol{E}_0 \exp(i\boldsymbol{k}\cdot\boldsymbol{r}_i - i\omega t) - \sum_{j\neq i} \boldsymbol{A}_{ij}\cdot\boldsymbol{P}_j \tag{2}$$

where $\boldsymbol{k}$ is the wave vector of the incident plane wave and the matrix $\boldsymbol{A}_{i,j}$ represents the interaction between all dipoles as given below

$$\boldsymbol{A}_{ij}\cdot\boldsymbol{P}_j = \frac{\exp(ik\boldsymbol{r}_{ij})}{\boldsymbol{r}_{ij}^{\,3}}\left\{k^2\boldsymbol{r}_{ij}\times(\boldsymbol{r}_{ij}\times\boldsymbol{P}_j) + \frac{(1-ik\boldsymbol{r}_{ij})}{\boldsymbol{r}_{ij}^{\,2}}\times [\boldsymbol{r}_{ij}^{\,2}\boldsymbol{P}_j - 3\boldsymbol{r}_{ij}(\boldsymbol{r}_{ij}\cdot\boldsymbol{P}_j)]\right\}, \qquad (j\neq i) \tag{3}$$

Once eq 2 has been solved by iteration with an initial guess of the unkown polarization $\boldsymbol{P}_j$, the extinction and absorption cross sections may be evaluated from the optical theorem:[32]

$$C_{\mathrm{ext}} = \frac{4\pi k}{|\boldsymbol{E}_0|^2}\sum_{j=1}^{N}\{\mathrm{Im}\}(\boldsymbol{E}_{\mathrm{inc},j}^{*}\cdot\boldsymbol{P}_j) \tag{4}$$

$$C_{\mathrm{abs}} = \frac{4\pi k}{|\boldsymbol{E}_0|^2}\sum_{j=1}^{N}\left\{\{\mathrm{Im}\}[\boldsymbol{P}_j(\alpha_j^{-1})^{*}\boldsymbol{P}_j^{*}] - \frac{2}{3}k^3|\boldsymbol{P}_j|^2\right\} \tag{5}$$

The scattering cross section is then obtained from $C_{\mathrm{sca}} = C_{\mathrm{ext}} - C_{\mathrm{abs}}$. As a discretization method for solving Maxwell's equations, DDA can be applied to any scattering problem of particles with arbitrary shape if we can generate the dipole array to represent the continuum target. The only requirement is that the interdipole separation d should be small compared to any structural dimensions of the target and the wavelength of light λ. More conservatively, the criterion is given by $|\boldsymbol{n}|kd < 1$, where $\boldsymbol{n}$ is the complex refractive index of the target material. For highly absorbing materials, like noble metals such as Au and Ag with a large extinction coefficient, better accuracy of the DDA calculation can only be achieved by using a large number of dipoles, thus reducing d. Target materials in a dielectric medium are efficiently considered by using a relative dielectric function of target to that of medium, which is reflected in the DDA calculation in the form of dipole polarizability.

There have been several different approaches to assign the dipole polarizabilities. Purcell and Pennypacker[26] used the Clausius−Mossotti relation, which is exact only in the static limit of $kd \rightarrow 0$. Draine and Goodman[33] made a significant modification on this and developed the prescription based on the lattice dispersion relation (LDR), which naturally includes the radiative reaction correction term and will be a good choice for finite dipole arrays as employed in our study.

Accuracy Test of DDA Calculation

In our current DDA calculations, the target geometries are approximated by a cubic array of point dipoles, so that it is necessary for the number of dipoles N to be large enough to reproduce a satisfactory target surface and thus diminish the inaccuracy originating from the surface granularity. However, because the computational effort scales with the volume of the system, there exists a limit in the number of dipoles that can be used. The optimum number N is somewhat arbitrarily taken as a number for which the numerical results converge to a certain value and change little by further increase in N.

The only conventional method to test the accuracy of DDA calculations is to compare the results for homogeneous isotropic

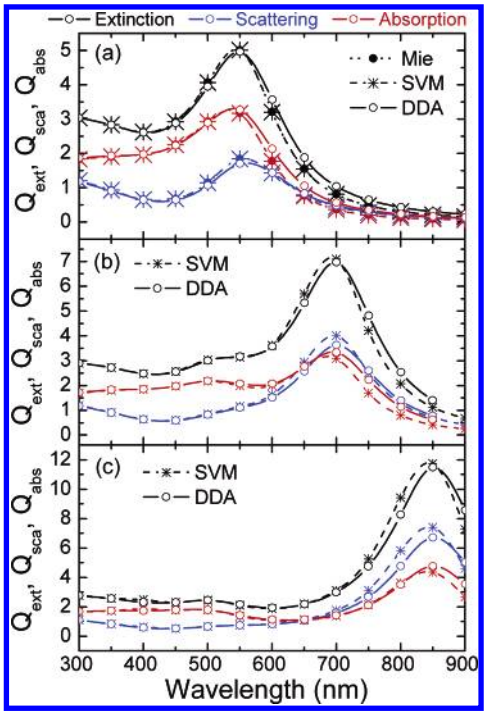

Figure 1. Calculated optical extinction, absorption, and scattering spectra (a) for a Au sphere with a radius of 40 nm in water and for a prolate Au spheroid with an aspect ratio R of (b) 2 and (c) 3, using different computational methods. The refractive index of water is approximated to be 1.34 for all wavelengths. Mie and SVM indicate the analytical solution of Maxwell's equation using the computational codes developed for sphere and spheroid, respectively. DDA shows the numerical solution using a discrete dipole approximation method where $N = 15515$ for sphere and $N = 28256$ and 42624 for the spheroid with $R = 2$ and 3, respectively. For spheroid, the effective radius of an equal volume sphere is assumed to have the same value of 40 nm.

spheres or spheroids with those of the exact analytical treatment. For this purpose, we carried out the analytical calculations for a sphere using the modified Bohren and Huffman code[32] based on Mie scattering theory and compared the results with the convergent solution of DDA. Figure 1a shows the comparison between the computational methods applied to the scattering problem of a Au sphere in water with a radius of 40 nm. Dielectric constants of Au are assumed to be the same as that of the bulk metal, which is obtained by a model fitting of the experimental data from Palik[34] using three Lorentz functions with a Drude term as suggested by Moskovits et al.[35] In all calculations, the refractive index of the surrounding medium is approximated to have a value of 1.34 at all wavelengths, close to that of water. From the figure, it is obvious that the overall DDA calculations are in great agreement with the results of the Mie theory although there is a little increasing discrepancy in the long wavelength region where the dielectric function of Au metal becomes large, inducing appreciable errors, as expected from the validity criterion mentioned above.

Another spectrum in Figure 1a was derived from the so-called "separation of variables method" (SVM),[23] which is one of the few analytical solutions of Maxwell's equations similar to Mie theory but extended for the scattering of spheroidal particles. For this calculation, we adopted the SVM code developed by Voshchinnikov and Farafonov,[23] and tested its validity using the aspect ratio (relative ratio of major optic axis to minor one, A/B) set to 1.001 for the spherical approximation. The results show excellent agreement with the Mie theory, which verifies that the SVM method is still very reliable even in the case of highly absorptive materials and thus applicable to the spheroidal Au particles for which further accuracy tests of DDA calculations were made.

Parts b and c of Figure 1 show the optical extinction, absorption, and scattering efficiencies computed by the DDA and the SVM methods for a spheroidal Au particle with a prolate geometry. The results are compared for two different aspect ratios, $R = 2$ and 3. It is common to specify the size of particles of an arbitrary shape and volume V as an "effective radius", $r_{eff} \equiv (3V/4\pi)^{1/3}$, which is the radius of a sphere having an equal volume to that of the particle. Throughout this paper, we fix the effective radius to be 40 nm otherwise the size is given, and characterized the case with fixed target orientation where the propagation direction of the incident light is assumed to be perpendicular to the optic axis of the prolate particle. Only two orthogonal polarizations of incident light are considered in all the calculations, one with a parallel electric field to the optic axis and one that is perpendicular to it.

The cross-sections C are related to the corresponding efficiency factors Q multiplied by the "viewing" geometrical cross-section G of the spheroids depending on the angle of incidence α between the propagation direction of light and the optic axis of the particle. In the case of oblique incidence ($\alpha \neq 0°$), the geometrical cross-section of a prolate spheroid is

$$G(\alpha) = \pi B(A^2 \sin^2 \alpha + B^2 \cos^2 \alpha)^{1/2} \qquad (6)$$

which is reduced to πAB in our case ($\alpha = 90°$). At this point, it should be noticed that the computational efficiencies represented here are actually the ratios of the cross-sections for spheroids to the geometrical cross-sections of the equal-volume spheres, πr_{eff}^2, and averaged over two polarizations, which is convenient for comparing the optical properties of the particles of different shapes. As seen in Figure 1b,c, both methods exhibit two well-known distinctive resonances corresponding to the transverse and the longitudinal mode of excitation of the surface plasmon, respectively. In the long wavelength region, the DDA calculation seems to give a somewhat red-shifted band and underestimates the scattering efficiency. However, the small deviation from the SVM results is thought to be acceptable as a reliable solution even in the spheroidal particles with a higher aspect ratio. Below, the DDA method is applied to investigate the various aspects with regards to the optical scattering of metal nanorods.

Effect of Shape Definition for Nanorod as a Function of Aspect Ratio

In most studies, the metal nanorods usually have been regarded as a prolate spheroid, which is certainly a good approximation. However, the most plausible geometry is a cylinder capped with two hemispheres, as illustrated in the inset of Figure 2b where the schematic geometries are represented for each case. So, we calculated the exact geometry of a Au nanorod and analyzed how much their computational efficiencies are dependent on the definition of their shape. Hereafter, we will just refer to the cylindrical particle capped with hemispheres as a nanorod.

Such a comparison was made as a function of aspect ratio when the effective radius of each geometry is fixed to have the same value (set as 40 nm throughout this study). This gives us a physical insight on how the shape definition actually affects the optical extinctions including absorption and scattering in the case where the total number of gold atoms that constitute the nanorod is kept the same. Parts a and b of Figure 2 show examples when $R = 2$ and 3, respectively. Note that the efficiencies represented here are also actually $GQ/\pi r_{eff}^2$, and

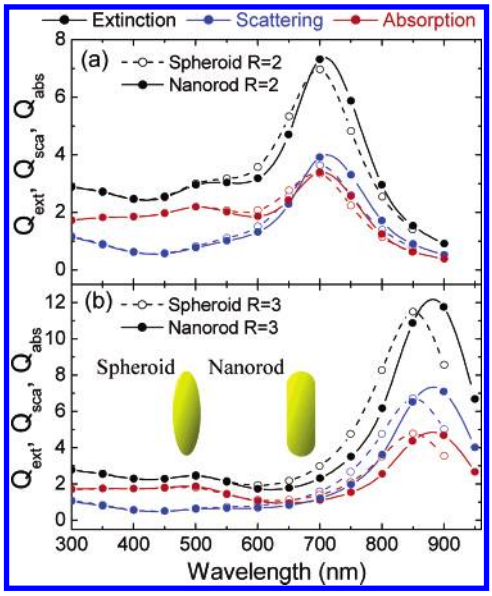

Figure 2. Comparison between the DDA results for Au metal nanoparticles with a prolate spheroid and a nanorod geometry. The effective radius r_{eff} was fixed to be 40 nm with an aspect ratio of (b) 2 and (c) 3. The inset of part b illustrates the two representative geometries of an elongated nanorod: (1) ellipsoidal spheroid and (2) cylinder capped with two hemispheres, both in prolate geometry. Hereafter, we just refer to the latter geometry as "nanorod"'.

the geometrical cross-section $G = 4a(b - a) + \pi a^2$ for a nanorod when $\alpha = 90°$. For a small aspect ratio, $R = 2$, both cases look a little different except for the noticeable enhancement in the scattering efficiency in the case of nanorod geometry. As the aspect ratio increases further, however, the optical spectra computed from both geometries become clearly distinguished from each other. It is also clear that the nanorod geometry induces a red-shift of the longitudinal plasmon resonance peak and scatters light more efficiently than the spheroidal particles.

With the nanorod geometry, the effect of the aspect ratio on the optical scattering and absorption efficiencies and their relative contributions to the total extinction were systematically investigated for Au metal nanoparticles. A series of calculated spectra are shown in Figure 3, where the variation of the longitudinal mode is observed to be apparent with increasing aspect ratio. Besides the well-known linear dependence of the longitudinal resonance wavelengths, as in the case of the ellipsoidal particles, the enhancement in the scattering efficiencies relative to the absorption is thought to be remarkable as the particle shape goes from a sphere to an elongated nanorod. For the quantitative analysis, the scattering quantum yield η is defined as

$$\eta = \left.\frac{Q_{sca}}{Q_{ext}}\right|_{Res} \tag{7}$$

which is the ratio of scattered efficiency to the total extinction at each resonance maximum. Figure 4 summarizes the dependence of resonance wavelength and radiative quantum yield of the longitudinal mode on the aspect ratio of Au nanorods. Unlike the resonance wavelength which shows a linear relationship with R, the scattering quantum yield changes in a somewhat complex manner. A slight elongation of Au nanosphere gives rise to a drastic increase in the relative scattering efficiency, which eventually reaches a maximum and begins to decrease with further increase in the aspect ratio, $R \geq 3.4$. Here, it should be emphasized that the scattering quantum yield can be considerably enhanced from 0.346 for a sphere up to 0.603 only by an elongational shape change, to an aspect ratio of 3, but keeping the volume of the nanoparticle (total number of gold atoms) constant.

Further elongation leads to a decrease in the scattering quantum yield. This may be explained by carefully looking at the formulas[23,32] which describe the optical scattering and absorption for a sphere and an extreme spheroid in a quasistatic approximation, and the wavelength dependent dispersion relationship of complex dielectric function of Au metal. Characteristics common to both formulas are that the optical scattering and absorption efficiencies are basically functions of the shape related parameter, i.e. aspect ratio and the materials dielectric function. Obviously, the resonance wavelength would be determined by the resonance condition, $|\epsilon_r + Y|^2 \rightarrow 0$, where ϵ_r is a relative dielectric constant of metal to surrounding medium ϵ_m/ϵ_s and Y is a parameter related to the particle shape. In addition, the absorption efficiency is approximately proportional to the imaginary part of the dielectric function of metal particles. Real and imaginary parts of the dielectric function of Au metal taken in this study are shown as a function of wavelength in Figure 5, where the data of Ag are also included for comparison. When the imaginary part of the dielectric function is negligibly small in the visible light region, as is typical for noble metals, the monotonically decreasing real part determines the resonance wavelength, which constitutes the origin of the linear relationship with respect to the aspect ratio. Interestingly, the imaginary part does not remain small but appears to increase gradually with increasing wavelength in the long wavelength region where the Drude free electron motion has the dominant effect. According to the Drude free electron model[36] (which describes the optical frequency dependent dielectric function of metal), ϵ_m is given by

$$\epsilon_m = \epsilon_1 + i\epsilon_2 = \epsilon_b - \frac{\omega_P^2}{\omega^2 - i\omega\Gamma} = \epsilon_b - \frac{\omega_P^2}{\omega^2 + \Gamma^2} + i\frac{\omega_P^2\Gamma}{\omega(\omega^2 + \Gamma^2)} \approx \epsilon_b - \frac{\omega_P^2}{\omega^2} + i\frac{\omega_P^2}{\omega^3}\Gamma \tag{8}$$

where ω, ω_P, and Γ mean optical and plasma frequencies, and damping constant (or collision frequency), respectively, and ϵ_b represents interband contribution. The imaginary part should have a tendency to increase with wavelength as the collision frequency of electrons in a metal becomes comparable to the optical frequency at the lower energy (longer wavelength region). This may be responsible for the observed decrease in the scattering quantum yield for nanorods with high aspect ratios which have longitudinal resonance absorption at longer wavelengths. At these wavelengths, the absorptive contribution is expected to increase due to the increase in the intrinsic dielectric function of the metal. Such an increase in the imaginary dielectric function of the metal is more significant for Au, which has a collision frequency $\Gamma_{Au} \sim 1.075 \times 10^{14}$ Hz, than for Ag with $\Gamma_{Ag} \sim 3.226 \times 10^{14}$ Hz,[36] as confirmed in Figure 5.

For the transverse mode, optical extinction spectra, deconvoluted for electric polarization of incident light perpendicular to the optic axis of the nanorod thereby excluding the possible overlapping effect from the multipolar excitation of the longitudinal resonance, are used to determine the scattering quantum yield and resonance wavelength as illustrated for a Au nanorod with $R = 1.6$ in Figure 6a. Parts b and c of Figure 6 summarize the dependence of resonance peak position and quantum yield of the transverse mode on the aspect ratio of Au nanorods. Quite

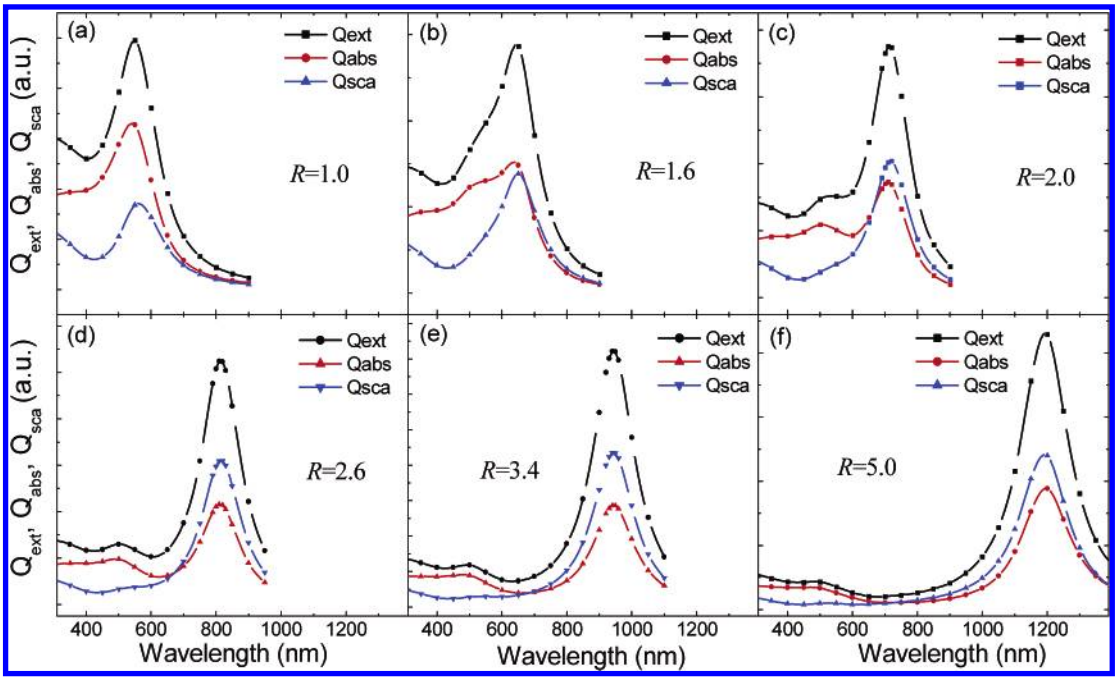

Figure 3. A series of calculated spectra for optical extinction, absorption, and scattering efficiencies for Au nanorods with different aspect ratios *R*. Here, the number of dipoles was taken to be 28256 for $R = 1$ and 57117 for $R = 5$.

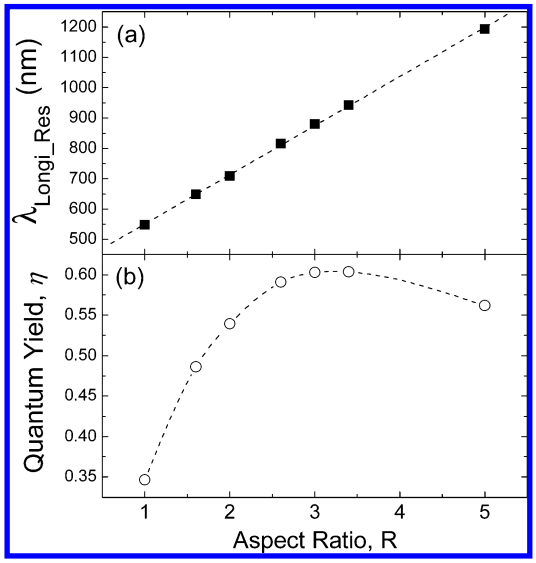

Figure 4. (a) Longitudinal surface plasmon resonance peak position and (b) radiative quantum yield η defined as a relative ratio of scattering efficiency to the total extinction, as a function of aspect ratio, *R*, for the Au metal nanorods in water ($n_s = 1.34$) with an effective radius of 40 nm.

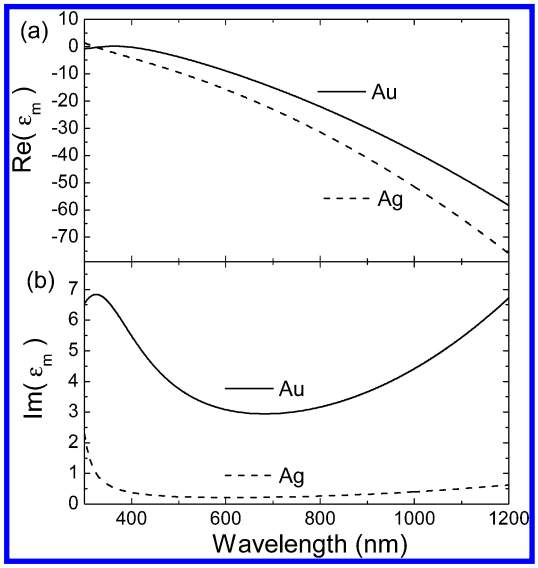

Figure 5. Wavelength-dependent dispersion of complex dielectric function for novel metals, Au and Ag, which was taken in our calculations.

different features are observed for the transverse mode. The resonance wavelength blue shifts and the scattering yield continuously decreases by increasing the aspect ratio. The longitudinal resonance wavelength shows the linear relationship with *R*, while the transverse does not. Sharing the viewpoint explained earlier for the longitudinal mode, the overall trends of the transverse mode are also interpreted by means of the variation in the dielectric function of the Au metal. In the short wavelength region of interest for the transverse mode, the interband transition has a dominant effect on the shape of the dielectric function of the Au metal and overlaps the transverse band. This results in an enlarged absorption related to the interband transition of electrons from the d-band to the s-band. However, the large magnitude of the imaginary dielectric function of metal plays a negative role on an excitation of plasmonic resonance, as manifested by the fact that the denominator $|\epsilon_r + Y|^2$ has a finite value, not approaching zero. As a result, the overall magnitude of the scattering and the absorption decreases as the aspect ratio increases. In addition, the resonance position is now determined not only by the real part of the dielectric function but also by the imaginary part, which makes the relationship with the aspect ratio nonlinear. This kind of interband effect is expected to be significantly suppressed in the case of Ag because silver has the energy threshold of the interband transition far from the plasmonic resonance region of interest, as seen in Figure 5. The computation for Ag metal nanorods is currently being processed.

Effect of Particle Size

The most effective way to enhance the scattering efficiency is simply by increasing the particle size, thereby enhancing the

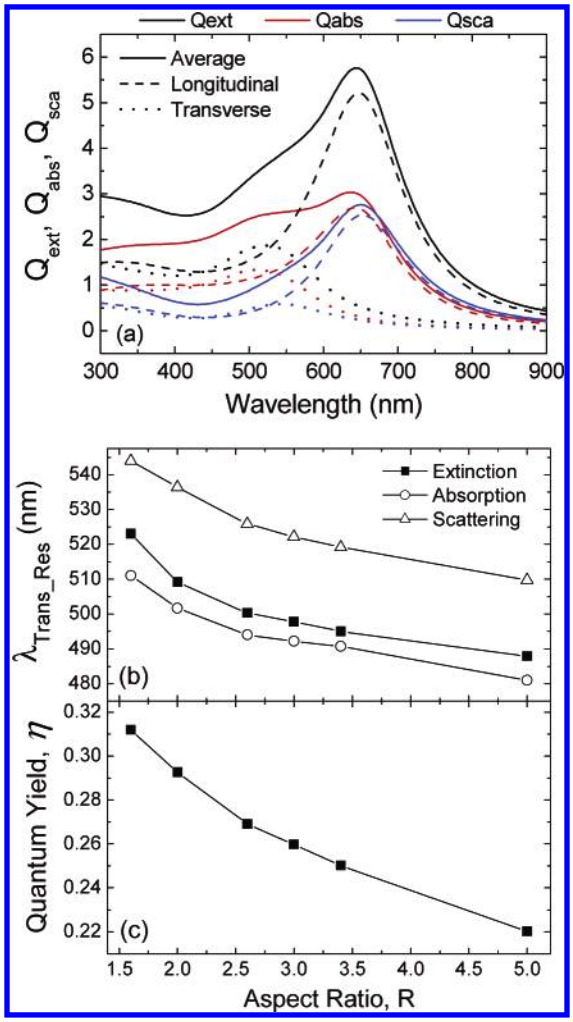

Figure 6. (a) Separation of the averaged optical spectra into the respective contribution from transverse and longitudinal resonance modes is demonstrated using the optical extinction spectra for a Au nanorod with $R = 1.6$, for example. Parts b and c show the resonance wavelength and radiative quantum yield as a function of R for the transverse mode, respectively.

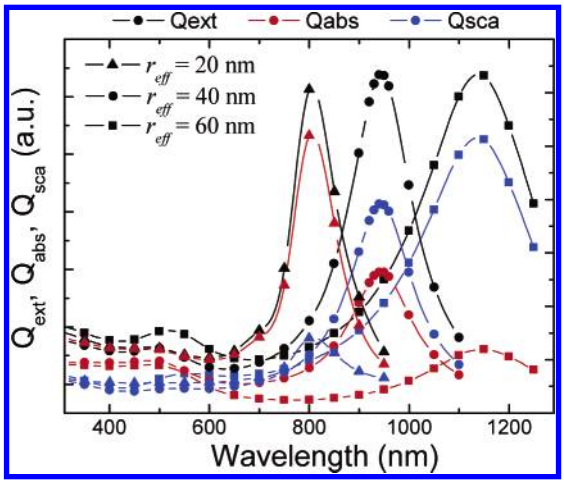

Figure 7. A series of calculated spectra for optical extinction, absorption, and scattering efficiencies of Au nanorods as a function of particle size at fixed $R = 3.4$.

volumetric radiative capacity, which is well-known in electrodynamics.[37] Figure 7 shows the calculated optical extinction spectra of Au metal nanorods with several different sizes (r_{eff} changes from 20 to 60 nm) at fixed $R = 3.4$. Note that the

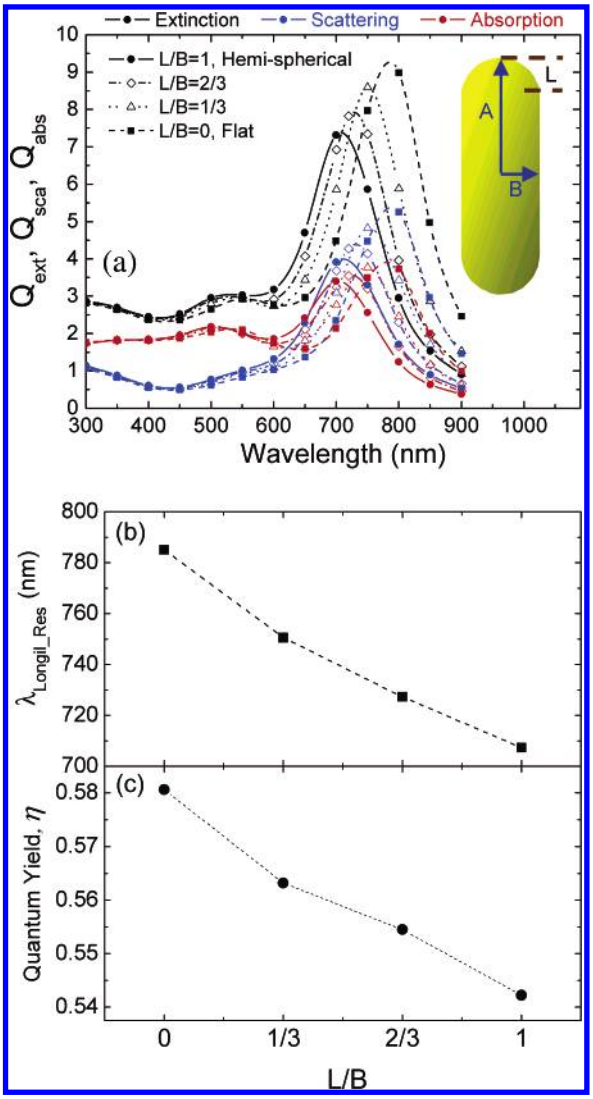

Figure 8. (a) Comparison of the DDA calculations as a function of end-cap shape factor, L/B, for the Au nanorods with $R = 3$. The inset of part a illustrates the end-cap shape definition. (b) Longitudinal surface plasmon resonance peak position and (c) radiative quantum yield η of a Au nanorod as a function of end-cap shape factor, L/B.

enhancement in the scattering efficiencies by such an increase in size is distinct but is definitely accompanied by an excessive broadening of the resonance due to extra damping mechanisms involved. It is found that the resonance wavelength of the longitudinal mode also changes showing a considerable redshift as well as a remarkable enhancement in the quantum yield.

Effect of End-Cap Shape

Our calculations were extended to a cylindrical nanoparticle to carefully investigate the effect of further modification of the end-cap shape on the optical scattering of metal nanorods. To do this, the shape of the Au nanorod with $R = 3$ was slightly modified by changing only the end-cap shape factor L/B from 1 for hemispherical end-cap to 0 for flat cylindrical particles, as defined in the inset of Figure 8a. Figure 8a shows the resultant spectra of the optical extinction, absorption, and scattering efficiencies with varying end-cap shape factor. It is observed that the total extinction is enhanced as the end-cap shape approaches a cylindrical particle with flat cap, which is mainly due to the increase in scattering efficiencies. The results are summarized in Figure 8b,c. By decreasing the curvature of the end-cap, i.e. approaching a flat surface, the resonance peak red-

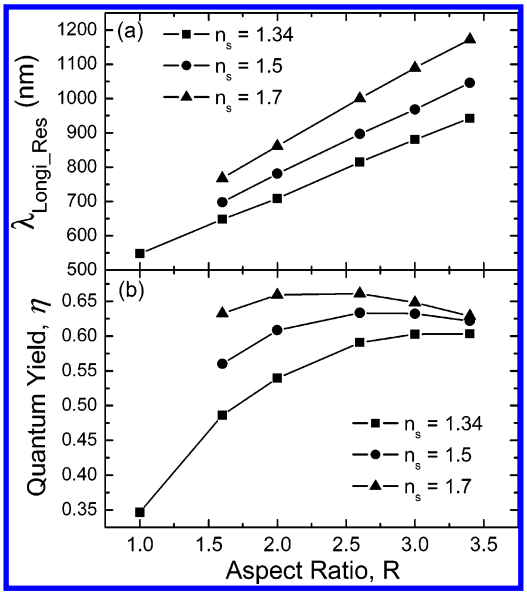

Figure 9. Effect of refractive index change of the surrounding medium on (a) the longitudinal resonance wavelength and (b) the scattering quantum yield η of a Au nanorod as a function of aspect ratio. r_{eff} was fixed to be 40 nm in all calculations.

shifts more and exhibits further enhancement in the optical scattering. This is very interesting because the intrinsic absorptive contribution was expected to be large due to the imaginary dielectric function of Au metal in this long wavelength region. This implies that the cylindrical geometry has a more significant contribution from the shape factor beyond the intrinsic effect from the dielectric function of Au metal.

Effect of Index of the Surrounding Medium

Information on how the optical scattering and absorption depend on the surrounding medium has practical application because it provides a fundamental mechanism for signal detection in applications such as biochemical sensors and local imaging. Therefore, it is very important to understand the dependence of the plasmonic resonance on the refractive index of the surrounding medium n_s. We simulated the effect of surrounding medium with a varying refractive index from 1.34 to 1.7, in which the Au metal nanorod, caped with hemispheres, is embedded. The effective radius of the Au nanorod is set at 40 nm. Figure 9 summarizes the results as a function of aspect ratio with varying the index of surrounding medium. A larger refractive index in the surrounding medium increases the wavelength of the longitudinal resonance and shows faster red-shift with an increase in the aspect ratio. For scattering quantum yield, a strong dependence on the aspect ratio was found. For a small aspect ratio, a small change in the medium refractive index results in a large variation in the relative contribution of optical scattering to the total extinction. However, as the aspect ratio of Au nanorods increases, the relative enhancement of the scattering efficiencies decreases with increasing the medium refractive index. This might be related to the faster bend-down in the quantum yield at higher n_s where the longitudinal resonance occurs at the longer wavelength.

Conclusions

We investigated the optical absorption and scattering, and their relative contributions to the total extinction of metal nanorods, using the discrete dipole approximation method. The accuracy and validity of the DDA calculations were verified by comparing the results with the well-known exact analytical solutions of Maxwell's equation derived with Mie theory for a sphere and a separation of variables method for a spheroid. The relative contribution of optical scattering to the total extinction of Au nanorods was found to greatly increase with a slight elongation of the sphere, i.e. as the aspect ratio R becomes slightly above 1 for particles having the same total number of gold atoms. The relative enhancement in the scattering efficiency then shows a slow saturation and finally the quantum yield decreases as R increases. It is thought that the larger red-shift in the resonance wavelength of the longitudinal mode with increasing aspect ratio should potentially accompany the larger absorptive contribution due to the intrinsic dielectric function of Au, especially the larger imaginary part. Although the easiest way to increase the scattering efficiencies is to increase the particle size, it is only possible at the expense of unwanted broadening of the resonance peak due to the more damping mechanisms involved. However, use of the nanorod shape benefits from the sharp resonance peak as well as excellent tunability. Interestingly, the relative contribution of scattering efficiency to total extinction was found to be enhanced further, as the nanorod shape goes from a spheroid to a cylindrical geometry. This implies that there exist two competing key factors, a weighting factor assigned to shape parameter and a dielectric function of the metal particle. This means that for the prolate nanoparticles, even if they have the same aspect ratio, its effect is certainly different depending on their exact geometry. In our case, the cylindrical geometry has more significant positive contribution from the shape factor for the enhancement of scattering efficiencies which overcomes the intrinsic negative effect from the dielectric function of Au metal up to a certain higher aspect ratio. Eventually above this aspect ratio, the absorptive contribution from the large imaginary dielectric function of Au would prevail.

Acknowledgment. This research was supported by the Material Research Division of the National Science Foundation (NSF) under grant No. 0138391. Computations were supported by the Center for Computational Molecular Science and Technology at the Georgia Institute of Technology and partially funded through a Shared University Research (SUR) grant from IBM and the Georgia Institute of Technology. We thank B. T. Draine and P. J. Flatau for use of their DDA code, DDSCAT 6.1. This research was also partly supported by a grant (code No.: 05K1501-02110) from "Center for Nanostructured Materials Technology" under "21st Century Frontier R&D Programs" of the Ministry of Science and Technology, Korea.

References and Notes

(1) McConnell, W. P.; Novak, J. P.; Brousseau, L. C., III; Fuierer, R. R.; Tenent, R. C.; Feldheim, D. L. *J. Phys. Chem. B* **2000**, *104*, 8925.
(2) Burda, C.; Chen, X.; Narayanan, R.; El-Sayed, M. A. *Chem. Rev.* **2005**, *105*, 1025.
(3) Kreibig, U.; Vollmer, M. *Optical Properties of Metal Clusters*; Springer: Berlin, Germany, 1995.
(4) Faraday, M. *Philos. Trans. R. Soc. London* **1857**, *147*, 145.
(5) Alivisatos, A. P. *Nat. Biotechnol.* **2004**, *22*, 47.
(6) Mirkin, C. A.; Letsinger, R. L.; Mucic, R. C.; Storhoff, J. J. *Nature* **1996**, *382*, 607.
(7) Haes, A. J.; Van Duyne, R. P. *Anal. Bioanal. Chem.* **2004**, *379*, 920.
(8) O'Neal, P.; Hirsch, L. R.; Halas, N. J.; Payne, J. D.; West, J. L. *Cancer Lett.* **2004**, *209*, 171.
(9) Maier, S. A.; Brongersma, M. L.; Kik, P. G.; Meltzer, S.; Requicha, A. A. G.; Atwater, H. A. *Adv. Mater.* **2001**, *13*, 1501.
(10) El-Sayed, I. H.; Huang, X.; El-Sayed, M. A. *Nano Lett.* **2005**, *5*, 829.
(11) Weissleder, R. *Nat. Biotechnol.* **2001**, *19*, 316.

(12) Loo, C.; Lin, A.; Hirsch, L.; Lee, M. H.; Barton, J.; Halas, N.; West, J.; Drezek, R. *Technol. Cancer Res. Treat.* **2004**, *3*, 33.
(13) Link, S.; Mohamed, M. B.; El-Sayed, M. A. *J. Phys. Chem. B* **1999**, *103*, 3073.
(14) Pérez-Juste, J.; Pastoriza-Santos, I.; Liz-Marzán, L. M.; Mulvaney, P. *Coord. Chem. Rev.* **2005**, *249*, 1870.
(15) Brioude, A.; Jiang, X. C.; Pileni, M. P. *J. Phys. Chem. B* **2005**, *109*, 13138.
(16) Yu, Y. Y.; Chang, S. S.; Lee, C. L.; Chris Wang, C. R. *J. Phys. Chem. B* **1997**, *101*, 6661.
(17) Coronado, E. A.; Schartz, G. C. *J. Chem. Phys.* **2003**, *119*, 3926.
(18) Sönnichsen, C.; Franzl, T.; Wilk, T.; von Plessen, G.; Feldmann, J.; Wilson, O.; Mulvaney, P. *Phys. Rev. Lett.* **2002**, *88*, 077402−1.
(19) Mie, G. *Ann. Phys.* **1908**, *25*, 377.
(20) Kerker, M.; Wang, D. S.; Giles, C. L. *J. Opt. Soc. Am.* **1983**, *73*, 765.
(21) Wu, Z. S.; Wang, Y. P. *Radio Sci.* **1991**, *26*, 1393.
(22) Asano, S.; Yamamoto, G. *Appl. Opt.* **1975**, *14*, 29.
(23) Voshchinnikov, N. V.; Farafonov, V. G. *Astrophys. Space Sci.* **1993**, *204*, 19.
(24) Mishchenko, M. I.; Travis, L. D.; Mackowski, D. W. *J. Quant. Spectrosc. Radiat. Transfer* **1996**, *55*, 535.
(25) Ludwig, A. C. *Comput. Phys. Commun.* **1991**, *68*, 306.
(26) Purcell, E. M.; Pennypacker, C. R. *Astrophys. J.* **1973**, *186*, 705.
(27) Kottman, J. P.; Martin, O. J. F.; Smith, D. R.; Schultz, S. *Opt. Express* **2000**, *6*, 213.
(28) Draine, B. T.; Flatau, P. J. *J. Opt. Soc. Am. A* **1994**, *11*, 1491.
(29) Jensen, T.; Kelly, L.; Lazarides, A.; Schatz, G. C. *J. Cluster Sci.* **1999**, *10*, 295.
(30) Kelly, K. L.; Coronado, E.; Zhao, L. L.; Schatz, G. C. *J. Phys. Chem. B* **2003**, *107*, 668.
(31) Yang, W. H.; Schatz, G. C.; Van Duyne, R. P. *J. Chem. Phys.* **1995**, *103*, 869.
(32) Bohren, C. F.; Huffman, D. R. *Absorption and Scattering of Light by Small Particles*; Wiley: New York, 1983.
(33) Draine, B. T.; Goodman, J. *Astrophys. J.* **1993**, *405*, 685.
(34) Lynch, D. W.; Hunter, W. R. In *Handbook of Optical Constants of Solids*; Palik, E. D., Ed.; Academic Press: New York, 1985; p 294.
(35) Moskovits, M.; Srnová-Šloufová, I.; Vlčková, B. *J. Chem. Phys.* **2002**, *116*, 10435.
(36) Simmons, J.; Potter, K. S. *Optical Materials*; Academic Press: San Diego, CA, 2000.
(37) Berestetskii, V. B.; Lifshitz, E. M.; Pitaevskii, L. P. *Quantum Electrodynamics*; Pergamon Press: Oxford, UK, 1982.